www.czasopisma.pan.pl PAN www.journals.pan.pl
Chemical and Process Engineering 2022, 43 (1), 57–80
DOI: 10.24425/cpe.2022.140811

Adsorption of n-hexane on a low-cost adsorbent obtained from waste tyres and its microwave regeneration

Tomasz Kotkowski, Robert Cherbański*, Eugeniusz Molga

Chemical and Process Engineering Department, Warsaw University of Technology,
ul. Waryńskiego 1, 00-645 Warszawa, Poland

This work investigates adsorption of n-hexane on activated tyre pyrolysis char (ATPC) and granular activated carbon (GAC) as a reference material in a fixed-bed column. Microwave-assisted regeneration is also considered. The adsorbed amount of n-hexane on ATPC is in the range of 37–58 mg/g. Microwave-assisted desorption of ATPC samples enables the recovery of up to 95% of adsorbed n-hexane in this non-optimized microwave setup with the efficiency of microwave energy conversion into heat of only 5–6%. For the 50% breakthrough time, ATPC and GAC are able to purify the n-hexane gas volumes in the ranges of 20–90 and 935–1240 cm^3/g, respectively. While adsorption kinetics is not satisfactorily described by pseudo-first and pseudo-second order kinetic models, it is very well reflected by a family of dynamic adsorption models, which are modelled with a single logistic function. Internal diffusion is likely the rate limiting step during adsorption on ATPC, while external and internal diffusion likely plays a role in adsorption to GAC. Although microwave-assisted regeneration is performed in a general purpose microwave reactor, both adsorbents show excellent performance and are very good candidates for the adsorption process. Preliminary results show that magnetite can further reduce microwave energy consumption.

Keywords: microwave regeneration, tyre pyrolysis char, granular activated carbon, n-hexane

1. INTRODUCTION

The utilization of waste tyres is a significant global concern and environmental challenge (ETRMA, 2019; World Business Council for Sustainable Development, 2008). An obvious consequence of automotive development is an increase in the amount of waste tyres. It is estimated that 1.4 billion end-of-life tyres (ELTs) are generated globally each year and around 4 billion ELTs had been deposited in landfills and stockpiles worldwide by 2008 (Acosta et al., 2016; Kandasamy and Gokalp, 2015; López et al., 2009; Sienkiewicz et al., 2012).

Pyrolysis of waste tires is considered an attractive alternative to traditional methods of waste tyre utilization, i.e. material and energy recovery. The process consists in the thermal decomposition of waste tyres in the absence of air, resulting in char (33%), oil (35%), gas (20%) and metal (12%) (Sharma et al., 1998). There is general agreement that pyrolysis char should be valorised to improve the economic viability of waste tyre pyrolysis (Antoniou et al., 2014). Such valorisation, being physical or chemical activation, improves the

* Corresponding author, e-mail: robert.cherbanski@pw.edu.pl

adsorption properties of the carbonaceous material by developing a porous structure within it (Antoniou et al., 2014; Mui et al., 2004).

To date, activated tyre pyrolysis chars (ATPCs) have been successfully applied for adsorption of different pollutants from the gas and aqueous phase (Kuśmierek et al. 2021a; Kuśmierek et al. 2021b).

In the present work n-hexane was chosen as a model adsorbate. As n-hexane emissions cause air pollution and significant damage to human health, including serious occupational neuropathies, they need to be controlled and minimised.

With a boiling point of 69 °C, n-hexane is recognized in the UE as a volatile organic compound (VOC) – "any organic compound having an initial boiling point less than or equal to 250 °C measured at a standard atmospheric pressure of 101.3 kPa." (Directive 2004/42/CE). The VOC emission is a serious environmental problem that is regulated in the EU by the Paints Directive (Directive 2004/42/CE) and the Industrial Emissions Directive (Directive 2010/75/EU).

Adsorption is the method of choice for dilute VOC streams. The method is the most common, cost-effective and well-established. Overall, absorption, condensation and membrane separation are also used for this purpose, but they are better suited for more concentrated VOC streams (Clean Air Technology, 1999).

A bottleneck in the adsorption process is the adsorbent regeneration step, which is usually time and energy consuming. In this context, microwave swing adsorption (MSA) is considered as an attractive alternative method to conventional temperature swing adsorption (TSA). MSA differs from TSA only in the regeneration step, which is accomplished using microwaves to heat the adsorbent bed instead of conventional heat supply methods. The main advantage of MSA compared to TSA is direct, instantaneous and selective heating. On the other hand, the major disadvantages of MSA include limited penetration depth of microwaves, hence limited depth of heating, and nonhomogeneous heating leading to hot-spots, i.e. local overheating (Cherbański and Molga, 2009).

To overcome these problems in industrial processes, various innovative technical solutions have been proposed. One of them is the Sairem series of professional LABOTRON™microwave reactors equipped with a patented internal transmission line technology (Stankiewicz and Nigar, 2020). In such reactors, microwaves are fed through a U-waveguide directly into the reaction mixture. Importantly, the reactor is made of stainless steel and equipped with a cooling jacket and a mechanical stirrer.

In addition, various microwave processes may suffer from non-uniform heating. Since higher microwave powers are applied for larger-scale processes, the problem of non-uniform heating is more pronounced here. To conquer this problem, several new reactor concepts have been proposed, namely: (1) monomodal microwave reactor from the Universities of Zaragoza and Valencia, (2) the rotating monolith catalyst from the University of Zaragoza and the Danish Technological Institute, and (3) traveling microwave reactor from Delft University of Technology (Stankiewicz and Nigar, 2020). Although these solutions are dedicated to reactors, they can also be adopted to adsorbers.

The first papers on the microwave regeneration of adsorbents come from the 1980s (Burkholder et al., 1986; Roussy and Chenot 1981; Roussy et al. 1984). To date, this technique has been successfully employed for the regeneration of various types of adsorbents, including silica gel (Polaert et al., 2010; Reuß et al., 2002; Robers et al., 2005), zeolites (Cha et al., 2004; Cherbański et al., 2011; Han et al., 2010; Kim and Ahn, 2012; Kim et al., 2007; Meier et al., 2009; Polaert et al., 2010; Price and Schmidt, 1998; Witkiewicz and Nastaj, 2014) and activated carbon (Ania et al., 2004; Ania et al. 2005; Ania et al., 2007; Çalişkan et al., 2012; Cha and Carlisle, 2001; Cha et al., 2004; Cherbański, 2018; Coss and Cha, 2000; Dehdashti et al., 2011; Fayaz et al., 2015; Foo and Hameed, 2012a; Foo and Hameed, 2012b; Foo and Hameed, 2012c; Hashisho et al., 2005; Liu et al., 2004; Mao et al., 2015b; Quan et al., 2004; Robers et al., 2005; Witkiewicz

and Nastaj, 2014; Yang et al., 2017). MSA was also the subject of several review papers (Bathen, 2003; Cherbański and Molga, 2009; Yuen and Hameed, 2009).

Although thermal regeneration can lead to deterioration of the adsorption capacity of activated carbons due to structural annealing (partial collapse of the porous structure) and formation of coke inside pores, the decrease of original adsorptive capacity is lower for MSR than for TSA (Ania et al., 2004; Ania et al., 2005). It is hypothesized that the diffusion of adsorbed molecules from the inside to the outside of an adsorbent is favoured because of the opposite temperature profile, which is characteristic for microwave heating (Ania et al., 2004; Ania et al., 2005). It is also likely that the direct interaction of microwaves with some polar compounds at low temperatures can lead to the thermal cracking of the adsorbed molecule inside the carbon porous network (Çalişkan et al., 2012). In contrast, there are several papers showing that the adsorption capacity was unaltered (Cha et al., 2004; Dehdashti et al., 2011; Fayaz et al., 2015; Foo and Hameed, 2012a; Foo and Hameed, 2012c; Mao et al., 2015a) or even higher (Ania et al., 2007; Liu et al., 2004; Quan et al., 2004) than the original adsorption capacity of activated carbon after several successive regeneration cycles of MSA. The unchanged adsorption capacity was also reported in the co-authors' previous work, in which regeneration of granular activated carbon (GAC) loaded with toluene was investigated by microwave and conductive regeneration (Cherbański, 2018).

This work concerns the adsorption of n-hexane on a low-cost adsorbent obtained from waste tyres with its subsequent regeneration by microwaves. While many research efforts have been made to study the adsorption of various pollutants on ATPC, previous works have neglected the adsorbent regeneration step. In the present paper, the intensified regeneration of ATPC is proposed by using microwaves. The influence of the various process operating conditions on adsorption and microwave desorption is thoroughly checked for ATPC and granular activated carbon (GAC) as a reference adsorbent. The following process operating conditions were tested: the impact of n-hexane vapour flow rate on breakthrough curves, the effects of microwave power and purge flow rate on microwave desorption and the influence of magnetite addition on microwave desorption.

The novel element in this work is the use of waste materials (TPC and ATPC) as VOC adsorbents in order to implement the strategy of sustainable development and environmental protection. While other works are mainly concerned with the sorption of pollutants from the aqueous phase on various waste materials, this work concerns adsorption from the gas phase. An additional novel element in this work is the microwave regeneration of these low-cost adsorbents, which allows for the intensification of the process.

2. EXPERIMENTAL

2.1. Materials

Granular activated carbon (GAC), purchased from Chempur (Poland), was used in the experiments as a reference adsorbent. Table 1 lists its selected physical and chemical properties.

The equivalent diameter of the ATPC particles is 18.4 μm, while the BET surface area is 256 m^2/g (Kotkowski et al., 2020).

n-Hexane (CAS: 110-54-3; purity ≥ 99.5%), purchased from Chempur (Poland), was used as an adsorbate. Nitrogen (purity ≥ 99.999%), delivered by Multax (Poland), was used as the carrier and purge gas.

Tyre pyrolysis char (TPC) was produced from shredded waste tyres of different types and brands in a pilot plant at our home university. A detailed description of this pilot plant can be found elsewhere (Kuśmierek

Table 1. Selected physical and chemical properties of GAC

Parameter	Value
Shape	cylindrical
Diameter	approx. 1 mm
Length	approx. 4 mm
Bulk density	454 g/dm^3
Moisture content	2.1 %
Methylene blue number	25 cm^3
Iodine number	997 mg/g
Water absorbability	0.88 cm^3/g

et al., 2020b). A batch of about 20 kg of waste tyres was pyrolyzed at 773 K under N_2 atmosphere. The TPC, oil and gas yielded 39 wt.%, 55 wt.% and 6 wt.%, respectively.

Activated tyre pyrolysis char (ATPC) was produced from the TPC feedstock in an electric tubular furnace under CO_2 atmosphere at 1373 K. The previous results of thermogravimetric analysis showed optimal activation temperature and time (Kotkowski et al., 2018). Employing these optimal conditions, a sample with the highest BET surface area (256 m^2/g) was fabricated and selected for further instigations of adsorption and microwave desorption.

2.2. Setups and procedures

Figure 1 shows the experimental setup used for adsorption of n-hexane vapour and microwave regeneration of the adsorption bed.

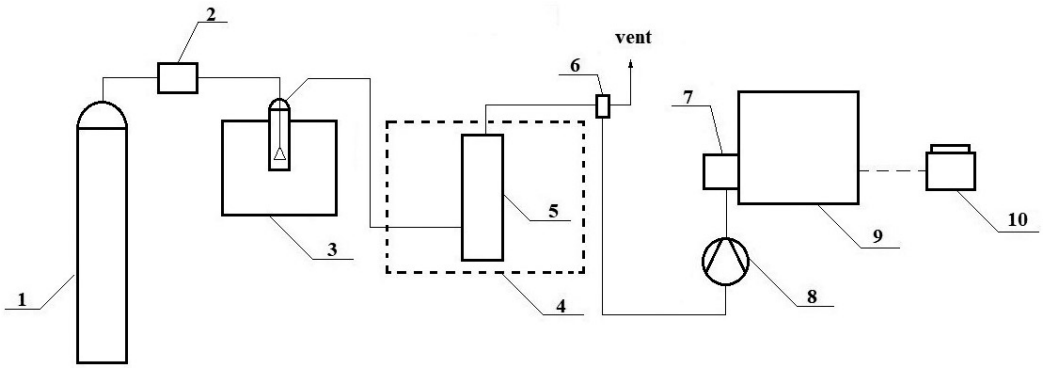

Fig. 1. Schematic diagram of the experimental setup for adsorption of n-hexane vapour. (1) Nitrogen cylinder, (2) mass flow controller, (3) thermostatic bath with bubbling gas saturator (used only in adsorption step), (4) a laboratory microwave oven (used only in microwave regeneration) (5) glass column with ATPC/GAC, (6) small capacity glass vessel from which the samples were taken for GC analysis and excess gas was vented, (7) two position valve, (8) peristaltic pump, (9) gas chromatograph, (10) personal computer

A detailed description of the experimental setups and the methods used for calibration, adsorption and microwave desorption can be found in the co-authors' previous work (Cherbański, 2018). All significant differences with respect to the current work are explained below.

Instead of using a simple glass vessel equipped with a polypropylene stopper and fibre optic (FO) sensors as in Cherbański (2018), a more customized quartz apparatus was designed and then made by a glassmaker (Fig. 2). The maximum operating temperature during the tests was limited by the FO sensors (type FOT-L-SD, FISO Technologies, Canada), which withstand temperatures up to 300 °C. Three FO sensors were slipped into the glass probes (i.d./o.d. is 1.7/3.7 mm) in such a way that each sensor's tip touched gently the bottom of the inner side of the glass probe. The length of the sensor's sensitive zone is 6.5 ± 0.5 mm and it starts 4 ± 1 mm from its tip. Gas was introduced into and evacuated form the apparatus by Teflon tubing. The carrier gas and the purge gas were evenly distributed through a perforated quartz plate that was fixed in the bottom part of the quartz apparatus. For ATPC/TPC, which was in a powder form, a layer of glass wool was placed in the upper part of the glass vessel to avoid elutriation of the material from the vessel. A Teflon clamp was used for the detachable connection of the cap and the vessel body. The quartz apparatus was placed in the centre of the multimode microwave cavity. The dimensions of this cavity can be found elsewhere (Cherbański and Rudniak, 2013). The microwave oven operated with a maximum power of 800 W at 2.45 GHz. The microwave power was adjustable with a setting accuracy of 1% (i.e. 8 W of microwave power). The Teflon tubing and FO sensors were inserted into the microwave cavity through a microwave choked outlet.

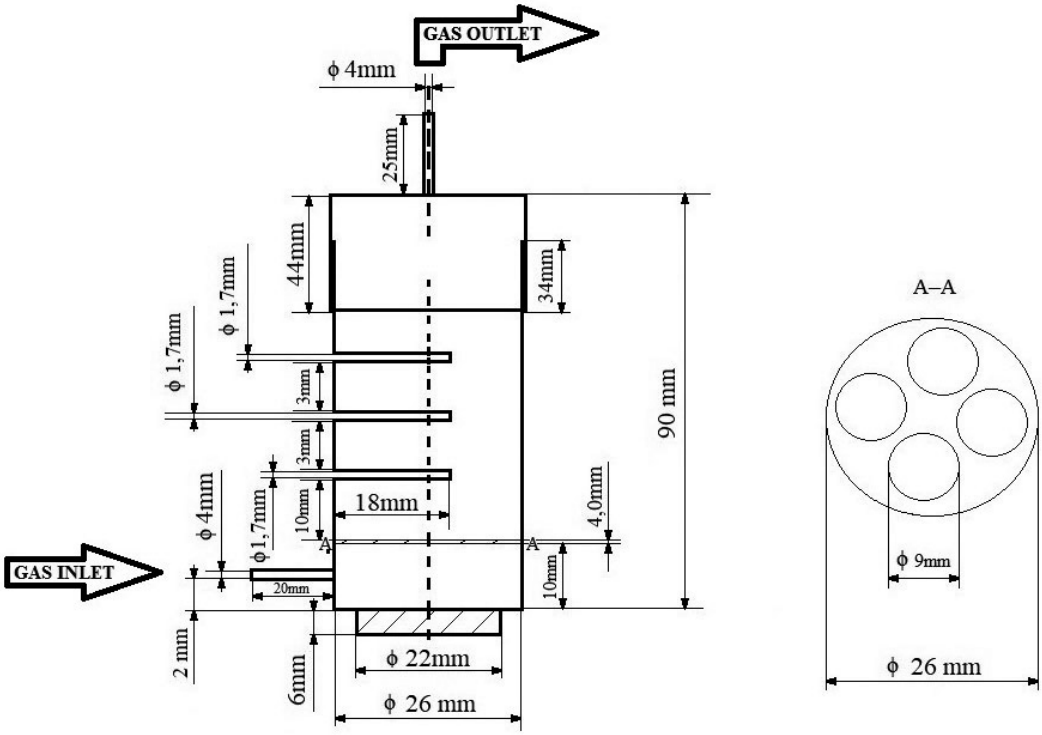

Fig. 2. A quartz vessel for adsorption and microwave desorption

Calibration was required to convert the chromatographic response of FID detector to the corresponding concentration of n-hexane vapour in the gas. The slope of the calibration curve (assuming a straight line) was calculated using the external method as proposed in (Cherbański, 2018). The resulting slope value was $2.48 \cdot 10^{-12}$ g/(cm^3 · mV · min) with the maximum relative error of 2.65%. Basically, adsorption and microwave regeneration were carried out using the same method as in (Cherbański, 2018).

The adsorbed and desorbed mass of n-hexane was calculated from Equations 1) and 2), respectively.

$$m_{\mathrm{ads}}(t) = \dot{V}_{\mathrm{N_2}}^{273.15} \frac{393.15}{273.15} Slope \int_0^t (Area_{\mathrm{MAX}} - Area)\, \mathrm{d}t \tag{1}$$

$$m_{\mathrm{des}}(t) = \dot{V}_{\mathrm{N_2}}^{273.15} \frac{393.15}{273.15} Slope \int_0^t Area \, \mathrm{d}t \tag{2}$$

where $\dot{V}_{\mathrm{N_2}}^{273.15}$ is the volumetric flow rate of the carrier/purge gas (N_2) at the normal temperature (displayed on the mass flow controller), the term $\dot{V}_{\mathrm{N_2}}^{273.15} 393.15/273.15$ is the volumetric flow rate of the carrier/purge gas recalculated for the temperature of 393.15 (the external sample loop temperature), *Slope* is the slope of the calibration curve, $Area_{\mathrm{MAX}}$ is the maximum signal of FID detector for the loaded adsorbent, *Area* is the chromatographic response of the FID detector.

A series of measurements was carried out. Tables 2 and 3 list the process conditions for all experiments.

3. ADSORPTION KINETICS

The pseudo-first-order (PFO) (Lagergren, 1898) and pseudo-second-order (PSO) models are very frequently used to describe adsorption kinetics. It is worth noting that the word 'kinetics' means in this context the rate of adsorption and should not be confused with the kinetic regime of mass transfer. In general, these models are essentially empirical equations (Rudzinski and Plazinski, 2007). However, when the overall adsorption rate is limited by external mass transfer resistance, adsorption kinetics can be often approximated by the pseudo-first-order model (Hubbe et al., 2019). On the other hand, when internal diffusion limits mass transport, adsorption rate can be often described by the pseudo-second-order kinetic model (Hubbe et al., 2019). The PFO and PSO models can be presented using the following differential equations, respectively.

$$\frac{\mathrm{d}q}{\mathrm{d}t} = k_1 \left(q_e - q\right) \tag{3}$$

where: q [mg·g^{-1}] is the amount of adsorbed n-hexane per unit mass of adsorbent, q_e [mg·g^{-1}] is the amount of adsorbed n-hexane per unit mass of adsorbent at equilibrium, k_1 [min^{-1}] is the pseudo-first order rate constant, and t [min] is the time.

$$\frac{\mathrm{d}q}{\mathrm{d}t} = k_2 \cdot \left(q_e - q\right)^2 \tag{4}$$

where: k_2 [g·mg^{-1}·min^{-1}] is the pseudo-second order rate constant, and the other symbols have the same meaning as in the PFO model.

After integration of Eqs. (3) and (4) and taking into account that q_e is known from the experiments, these equations can be rewritten in the alternative forms for the PFO and PSO models, respectively (Simonin, 2016).

$$\frac{q}{q_e} = 1 - e^{(-k_1 t)} \tag{5}$$

$$\frac{q}{q_e} = \frac{k_2^* t}{1 + k_2^* t} \tag{6}$$

where $k_2^* \equiv k_2 q_e$.

Please note that while adsorption kinetics is commonly modelled using the PFO and PSO models, they are essentially empirical equations that make little physical sense. For instance, Plazinski et al. (2009) found that the PSO model does not correspond to any specific situation, but rather is able to fit typical adsorption data as an approximation. There is general agreement, however, that the often observed perfect fit of adsorption data to the PSO model is due to surface reactions or internal diffusion, which are the rate limiting steps in these cases.

Table 2. Details of performed experiments for GAC. The mass of the outgassed adsorbent for adsorption was 13.16 g for all experiments except for GAC 1–2, for which it was 13.15 g. For GAC 15, 1.44 g of magnetite was added

Experiment symbol	Adsorption			Desorption			
	Nitrogen flow rate during adsorption [Nml/min]	Adsorbed amount [mg/g]	Relative error (Eq. (9)) [%]	Nitrogen flow rate during regeneration [Nml/min]	Microwave power [W]	Microwave energy [kJ]	Regeneration degree (GC) [%]
Reproducibility of the results							
GAC 1	200	325	3.58	200	32	460.8	83.85
GAC 2	200	303	8.13	200	32	460.8	88.37
GAC 3	200	320	7.77	200	32	460.8	86.24
Effect of carrier gas flow rate on the breakthrough curves							
GAC 4	100	378	12.36	–	–	–	–
GAC 5	150	319	1.41	–	–	–	–
GAC 3	200	320	7.77	200	32	460.8	86.24
GAC 6	250	296	9.86	–	–	–	–
GAC 7	300	336	0.42	–	–	–	–
GAC 8	350	282	14.75	–	–	–	–
GAC 9	400	299	7.67	–	–	–	–
Effect of microwave power on desorption							
GAC 10	200	336	1.09	200	16	460.8	79.88
GAC 11	200	351	4.93	200	24	460.8	78.48
GAC 3	200	320	7.77	200	32	460.8	86.24
Effect of purge flow rate on desorption							
GAC 12	200	328	1.30	100	32	460.8	81.66
GAC 3	200	320	7.77	200	32	460.8	86.24
GAC 13	200	327	0.75	300	32	460.8	92.36
GAC 14	200	342	2.93	400	32	460.8	89.61
Effect of magnetite on desorption							
GAC 10	200	336	1.09	200	16	460.8	79.88
GAC 15	200	322	4.77	200	16	230.4	74.73

On the other hand, the diffusion models, as the intraparticle model of Weber and Morris (1963), are generally based on equations obtained from solving Fick's laws of diffusion and can therefore be helpful to check whether internal diffusion limits the adsorption process.

Table 3. Details of performed experiments for ATPC/TPC. The mass of the outgassed adsorbent for adsorption was 13.16 g for all experiments

Experiment symbol	Adsorption			Desorption			
	Nitrogen flow rate during adsorption [Nml/min]	Adsorbed amount [mg/g]	Relative error (Eq. (9)) [%]	Nitrogen flow rate during regeneration [Nml/min]	Microwave power [W]	Microwave energy [kJ]	Regeneration degree (GC) [%]
Reproducibility of the results							
TPC 1	200	42	9.80	–	–	–	–
TPC 2	200	30	3.10	–	–	–	–
TPC 3	200	25	4.64	–	–	–	–
Effect of n-hexane vapour flow rate on the breakthrough curves							
TPC 4	100	28	8.23	–	–	–	–
TPC 1	200	42	9.80	–	–	–	–
TPC 5	300	29	3.62	–	–	–	–
TPC 6	400	34	9.79	–	–	–	–
ATPC 1	100	37	3.17	–	–	–	–
ATPC 2	200	58	9.28	200	32	172.8	80.45
ATPC 3	300	37	0.80	–	–	–	–
ATPC 4	400	44	0.94	–	–	–	–
Effect of microwave power on desorption							
ATPC 5	200	38	2.83	200	16	86.4	85.33
ATPC 6	200	40	7.45	200	24	129.6	94.90
ATPC 2	200	58	9.28	200	32	172.8	80.45
Effect of purge flow rate on desorption							
ATPC 7	200	40	5.28	100	32	172.8	90.61
ATPC 2	200	58	9.28	200	32	172.8	80.45
ATPC 8	200	46	1.55	300	32	172.8	92.80
ATPC 9	200	50	2.36	400	32	172.8	92.02

The IP model can be written in the following form

$$q(t) = K_p \cdot \sqrt{t} + C \tag{7}$$

where: K_p [mg·g^{-1}·s$^{0.5}$] is the IP model rate constant, C [mg·g^{-1}] is the constant connected with the boundary layer thickness (i.e. the film thickness for the external film diffusion model), $q(t)$ [mg·g^{-1}] is the amount of adsorbed n-hexane per unit mass of adsorbent at time t [min].

A higher value of C indicates a thicker boundary layer, which is linked with a greater external diffusion resistance. Overall, when the plot $q(t)$ versus $\sqrt{t}$ is linear and goes through the origin, it means that internal diffusion controls the adsorption process. In the case of materials with a well-developed internal structure, multi-linearity can be observed in such a plot, showing that adsorption occurs with different rates when adsorbate molecules move from the wider pores towards the narrower pores (macropores → mesopores → micropores) (Wu et al., 2009).

There are also several dynamic adsorption models very often used to describe breakthrough curves, as the Thomas (Th) (Wang et al., 2015), Yoon–Nelson (Y–N) (Han et al., 2019; Wang et al., 2015; Wang et al., 2021; Yoon and Nelson, 1984; Zhang et al., 2018), Bohart–Adams (B–A) (Bohart and Adams, 1920; Yan et al., 2018) models. Indeed, they are quite simple and can be rearranged into the same logistic function (Chatterjee and Schiewer, 2011; Chu, 2020; Tan and Hameed, 2017; Yan et al. 2018) as shown below

$$\frac{C_t}{C_0} = \frac{1}{1 + e^{(a-bt)}} \tag{8}$$

where the a and b coefficients are explained in Table 4.

Table 4. Meaning of the logistic function coefficients used to model adsorption dynamics

Model	a	b	Remark
Thomas (Wang et al., 2015)	$a = k_{\mathrm{Th}} q_e \frac{m}{Q}$	$b = k_{\mathrm{Th}} C_0$	k_{Th} [ml·mg^{-1}·min^{-1}] – the Thomas rate constant, q_e [mg·g^{-1}] – the equilibrium adsorption capacity, m [g] – the amount of absorbent in the column, Q [ml·min^{-1}] – the vapour flow rate
Yoon–Nelson (Han et al., 2019; Wang et al., 2015; Wang et al., 2021; Yoon and Nelson, 1984; Zhang et al., 2018)	$a = k_{\mathrm{YN}} \tau$	$b = k_{\mathrm{YN}}$	k_{YN} [min^{-1}] – the Yoon–Nelson rate constant, τ [min] – is time required to reach $C_t/C_0 = 0.5$
Bohart–Adams (Bohart and Adams, 1920)	$a = k_{\mathrm{BA}} N_0 \frac{X}{V}$	$b = k_{\mathrm{BA}} C_0$	k_{BA} [ml·mg^{-1}·min^{-1}] – the Bohart–Adams rate constant, N_0[mg·ml^{-1}] – the adsorptive capacity of the adsorbent, X [cm] – the bed height, V [cm·min^{-1}] is the superficial velocity of eluent

4. RESULTS AND DISCUSSION

The reproducibility of the results obtained with the proposed experimental method was checked by performing three independent series of experiments for GAC and TPC under the same conditions, and then comparing the obtained results (GAC 1–3, Table 2 and TPC 1–3, Table 3). Although some discrepancies between the curves can be observed for adsorption and microwave desorption (Fig. 3), the reproducibility of the results is rather good.

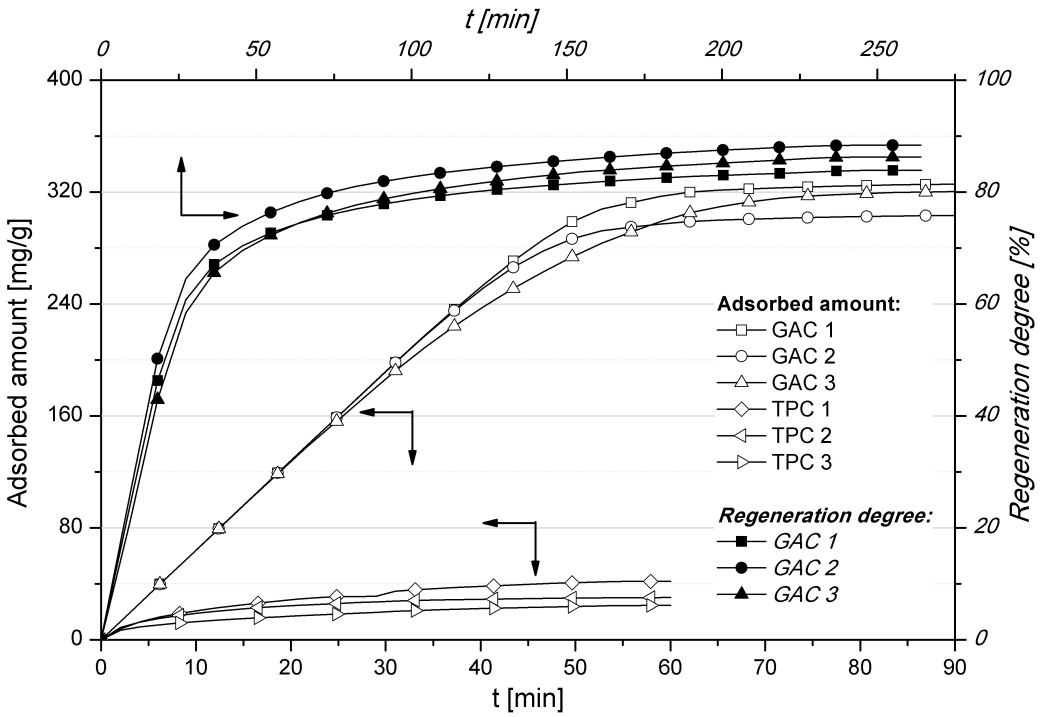

Fig. 3. Reproducibility of the results for the adsorption and desorption of n-hexane. The tests performed at the same conditions (No. 1–3, Table 2)

To check whether the chromatographic method provides consistent results with the weight measurements, relative errors were calculated for all samples shown in Tables 2 and 3. The relative errors were calculated with the following equation.

$$\text{RelError} = \frac{\left| m^{GC}_{\text{hex,ads}} - m^{\text{weight}}_{\text{hex,ads}} \right|}{m^{\text{weight}}_{\text{hex,ads}}} 100\% \tag{9}$$

The calculated errors were below 10% for most samples. Only two GAC samples showed higher errors (Table 2). Moreover, almost the same mean errors for the GAC and ATPC/TPC samples were obtained, amounting to 5.7% and 5.6%, respectively. On the basis of a separate weight measurement, the maximum adsorbed amount of n-hexane on the layer of glass wool was about 2% of that for TPC. Therefore, this contribution was considered to be negligible. In conclusion, the chromatographic method has been positively validated as suitable for tracking adsorption/desorption dynamics.

Figure 4 shows the effect of carrier gas flow rate on the adsorption kinetics. It is apparent from the figure that the uptake of n-hexane on GAC is faster when the carrier gas flow rate is higher. Generally, this is due to two main factors that will be discussed later. On the other hand, the flow rate apparently has no effect on the q/q_e ratio for the ATPC samples.

Table 5 presents the results of modelling the adsorption kinetics using PFO and PSO models. It shows the parameter values with the associated standard errors and the adjusted coefficients of determination, $\overline{R}^2$. The fit of the PFO and PSO models (Fig. 4) and the $\overline{R}^2$ values (Table 5) reveal that the PFO model performs better than the PSO model. However, the agreement between the experimental and modelling results is rather disappointing, even for the PFO model.

The IP model was used to test whether internal diffusion is the rate-limiting step in some experiments. As can be seen in Figure 5, this is very likely for all ATPC samples, which follow a straight line through the origin on the plot. More specifically, these experimental data are even better described using segmented regression with two linear segments. Such performance can be explained by the decreasing diffusion rate

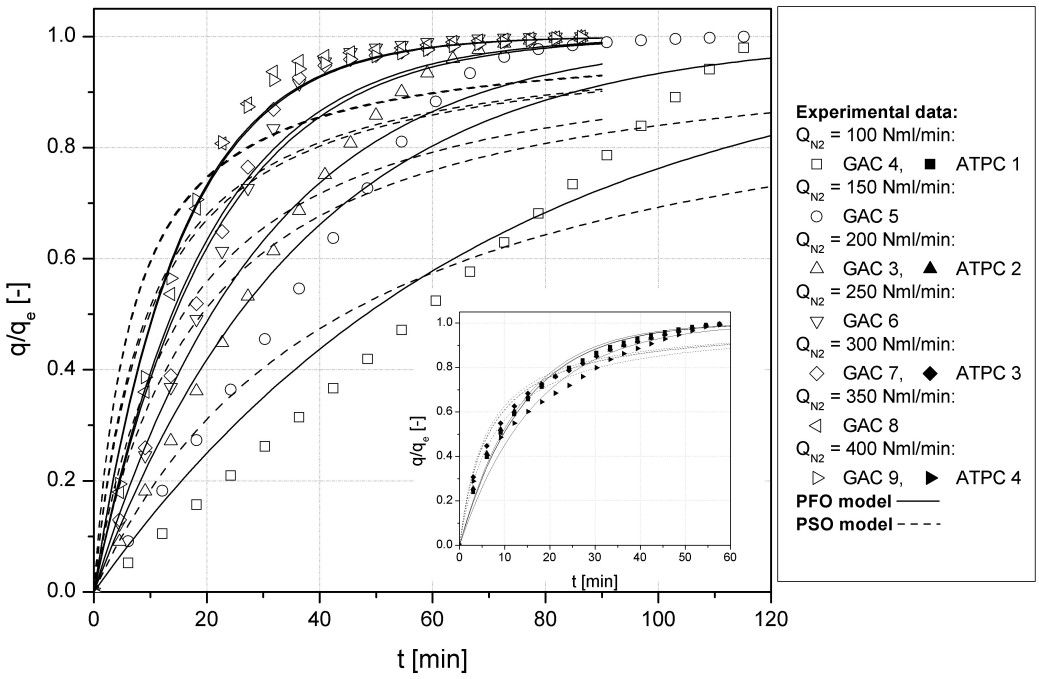

Fig. 4. The effect of carrier gas flow rate on the ratio q/q_e for the GAC and ATPC samples. The symbols refer to experimental data, while the solid and dashed lines refer to the PFO and PSO models

Table 5. Parameter values for the PFO and PSO models

Sample	Nitrogen flow rate [Nml/min]	PFO			PSO		
		k_1 [min^{-1}]	Standard error	$\overline{R}^{2*)}$	k_2^* [min^{-1}]	Standard error	$\overline{R}^{2*)}$
GAC 4	100	0.01437	$2.90 \cdot 10^{-4}$	0.960	0.02251	0.00133	0.831
GAC 5	150	0.02707	$6.30 \cdot 10^{-4}$		0.05236	0.00368	
GAC 3	200	0.03335	$7.53 \cdot 10^{-4}$		0.06332	0.00433	
GAC 6	250	0.04831	0.00128		0.10136	0.00805	
GAC 7	300	0.05014	0.00135		0.10588	0.00854	
GAC 8	350	0.06519	0.00200		0.14565	0.01325	
GAC 9	400	0.06608	0.00204		0.14787	0.01353	
ATPC 1	100	0.0711	0.0011	0.975	0.15579	0.00595	0.932
ATPC 2	200	0.07166	0.00111		0.15797	0.00607	
ATPC 3	300	0.07457	0.00118		0.16855	0.00663	
ATPC 4	400	0.06017	$8.60 \cdot 10^{-4}$		0.1301	0.00467	

*) The adjusted coefficient of determination, $\overline{R}^2 = 1 - \frac{RSS/df_{\text{Error}}}{TSS/df_{\text{Total}}}$ where RSS is the residual sum of squares, TSS is the total sum of squares, df is degree of freedom (OriginLab Corporation, 2021).

as the adsorbate molecules move from wider to narrower pores within the adsorbent. On the other hand, it is likely that both resistances, i.e. external and internal diffusion play a role during adsorption process on GAC as all these curves are highly non-linear.

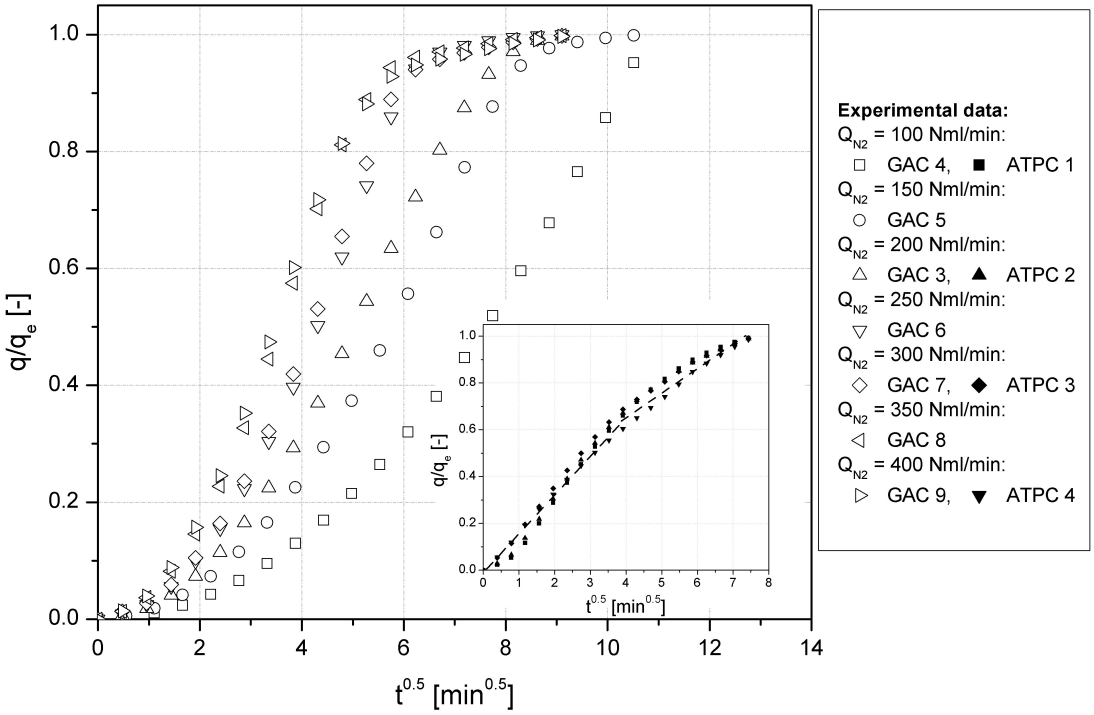

Fig. 5. Testing the mass-limiting step during adsorption with the IP model

Figure 6 presents the breakthrough curves for the GAC and ATPC samples. By multiplying the breakthrough times by the corresponding carrier gas flow rates, the total purified gas volume can be calculated; in the case of GAC samples, the breakthrough times are determined using a ratio of $C/C_0 = 0.05$. These simple calculations show that the process is more efficient when the carrier gas flow rate is lower. Such performance

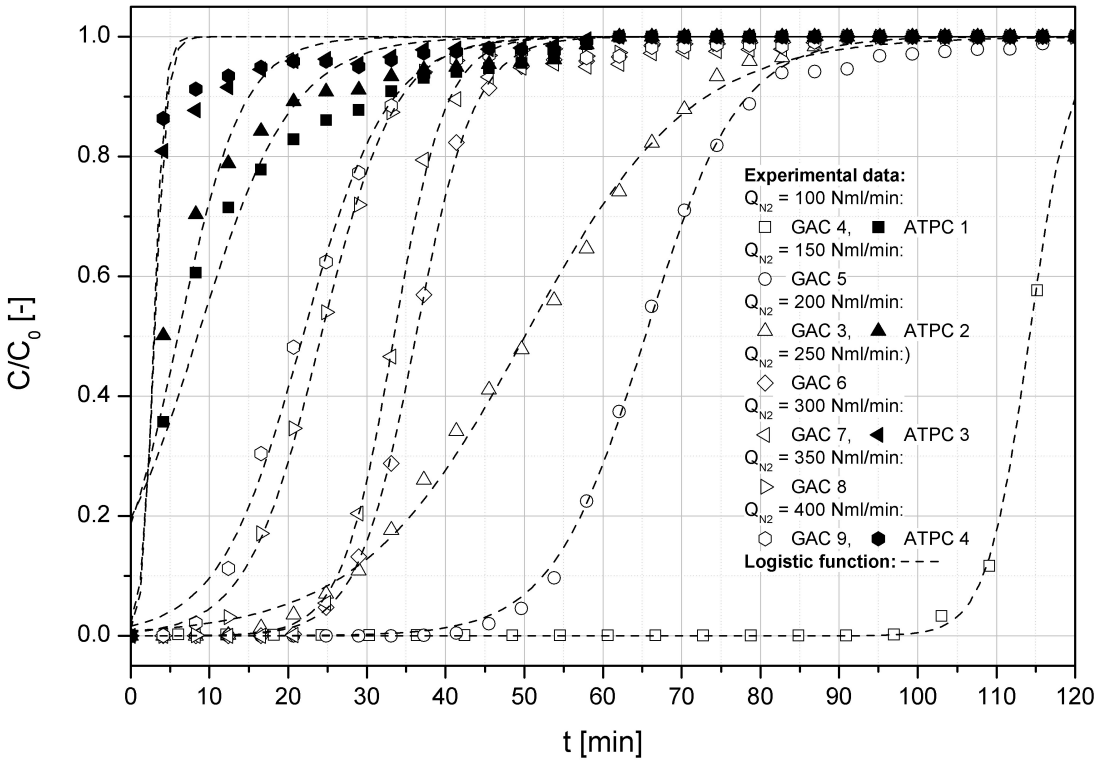

Fig. 6. The effect of carrier gas flow rate on the breakthrough curves for GAC and ATPC. The symbols mean experimental data, while the dashed lines mean the logistic function model

can be explained on the basis of a simple analysis presented below. Note, however, that the analysis applies only for the GAC samples showing the effect of external diffusion on the process.

Using a general correlation for mass transfer coefficient

$$Sh = A\,\mathrm{Re}^{e}\,Sc^{f} \tag{10}$$

and then rewriting Eq. (10) as

$$Sh = \frac{k_c \cdot d_h}{D_{AB}} = A\left(\frac{u_0 d_h}{\nu}\right)^{e} Sc^{f} \tag{11}$$

one can obtain the following relationship

$$k_c = K \cdot u_0^{e} \tag{12}$$

where k_c is the mass transfer coefficient, K is the proportional constant, u_0 is the superficial velocity, e is the constant, which is generally lower than 1, d_h is the hydraulic diameter of particles, D_{AB} is the diffusion coefficient, ν is the kinematic viscosity of gas phase.

Dividing Eq. (12) by u_0, we get

$$\frac{k_c}{u_0} = K \cdot u_0^{e-1} = \frac{K}{u_0^{1-e}} \tag{13}$$

Given that $e < 1$ for laminar and turbulent flows, it is clear that increasing the carrier gas flow rate, which means also increasing its superficial velocity, leads to a decrease of the k_c/u_0 ratio. In other words, the increase of the mass transfer coefficient due to the higher carrier gas flow rates becomes less pronounced at higher flows, while the shorter residence time of the gas in the column becomes the decisive factor. As the residence time becomes too short, the adsorbent bed height cannot be used effectively. In conclusion, the lower the flow rate, the GAC adsorbent bed can be utilized more effectively.

As far as the ATPC samples are concerned, the breakthrough times are very low and hardly distinguishable. Therefore, the times corresponding to the ratio of $C/C_0 = 0.5$ were used to calculate the volume of the gas purified by ATPCs. It is worth noting that the influence of the flow rate discussed for the GAC samples should not determine the adsorption rate in the case of ATPC samples for which the influence of internal diffusion is postulated. However, an unequivocal statement of this fact on the basis of the breakthrough curves is not possible. Using these times, the volumes which could be purified by GAC and ATPC are in the range of 20–90 cm^3/g and 935–1240 cm^3/g, respectively.

Table 6 shows the parameter values with the associated standard errors and the adjusted coefficients of determination, $\overline{R}^2$, for a logistic function, which was used to model the breakthrough curves. Note that the found logistic functions are in good agreement with the experimental data and approximate the data much better that the PFO and PSO models.

Figures 7 and 8 display the effect of microwave power on desorption for GAC and ATPC, respectively.

Remote and direct interaction of microwaves with matter is one of the main advantages of microwave heating. Note that conventional heat supply methods require an external heat source. Heat is typically transferred to the adsorbent bed through the adsorber wall or, more commonly, by preheated purge gas. A rapid heating rate is observed when the dielectric properties of the heated material ensure a high dissipation rate of microwave energy, as for the tested samples. Note that the boiling point of n-hexane (69 °C) in the middle position of the GAC bed was already attained after 34 min, 7 min, 2.5 min for the microwave power of 16 W, 24 W, and 32 W, respectively. Even shorter times were accomplished for the ATPC bed at the same positions of FO sensors, showing 6 min, 3 min, 2.5 min for the microwave power of 16 W, 24 W, and 32 W, respectively. Similarly, very fast cooling can be observed after switching off the microwave power in Figs. 7 and 8.

Table 6. Parameter values of the logistic function used to model adsorption dynamics

Sample	Nitrogen flow rate [Nml/min]	Logistic function				
		a [–]	Standard error	b [min^{-1}]	Standard error	$\overline{R}^2$
GAC 4	100	42.61648	1.40259	0.37324	0.01232	0.99387
GAC 5	150	11.07185	0.01232	0.16937	0.84549	
GAC 3	200	4.77785	0.84549	0.09539	0.01291	
GAC 6	250	9.75185	0.01291	0.26924	0.22417	
GAC 7	300	10.22305	0.22417	0.30567	0.00437	
GAC 8	350	5.19064	0.00437	0.21466	0.87968	
GAC 9	400	4.11278	0.87968	0.188	0.02421	
ATPC 1	100	1.41285	0.02421	0.16645	1.00451	
ATPC 2	200	1.47036	1.00451	0.24476	0.02996	
ATPC 3	300	3.85366	0.02996	1.27575	0.36643	
ATPC 4	400	4.41095	0.36643	1.51018	0.01486	

*) The adjusted coefficient of determination, $\overline{R}^2 = 1 - \frac{RSS/df_{\text{Error}}}{TSS/df_{\text{Total}}}$ where RSS is the residual sum of squares, TSS is the total sum of squares, df is degree of freedom (OriginLab Corporation, 2021).

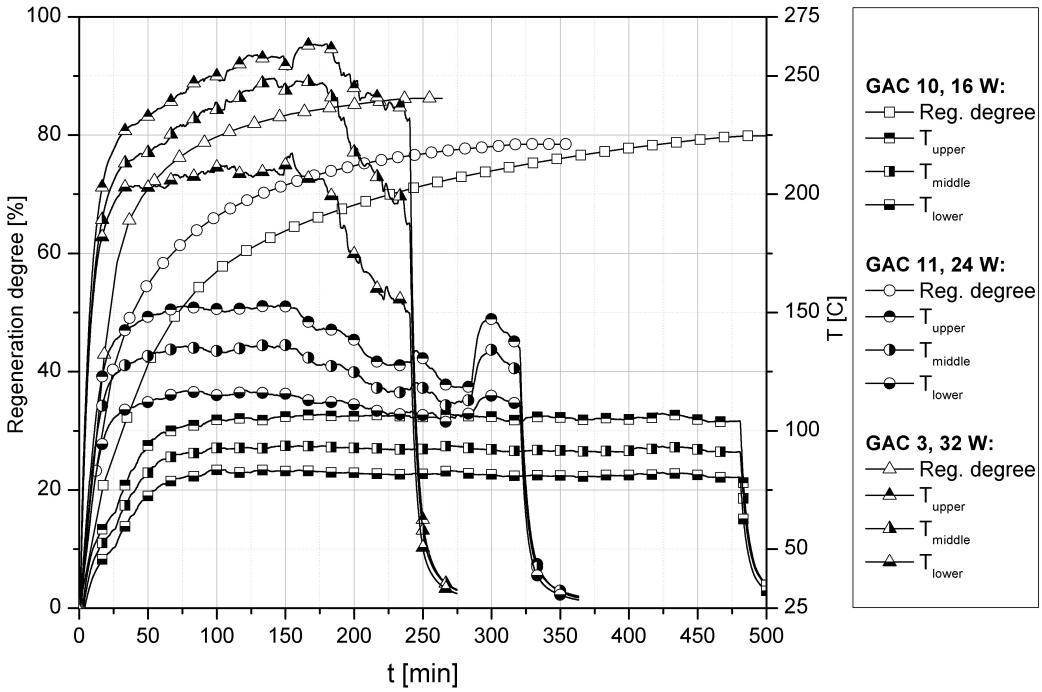

Fig. 7. Effect of microwave power on desorption for GAC

Although the high efficiency of microwave heating is partly due to hot-spot formation or local overheating, it also leads to non-homogeneous heating. In the case of the GAC bed, the greatest differences between the temperatures measured in the upper and lower positions of the FO sensors are about 24 °C, 37 °C, 81 °C for the microwave power of 16 W, 24 W, and 32 W, respectively. In relation to the ATPC bed, the greatest

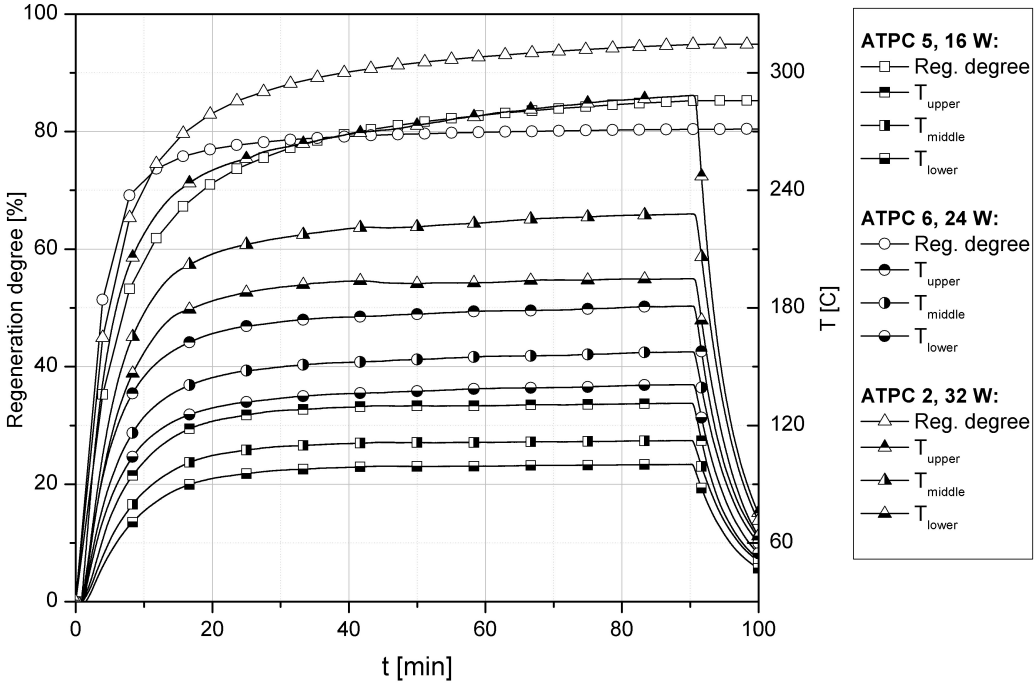

Fig. 8. Effect of microwave power on desorption for ATPC

differences are about 31 °C, 40 °C, 93 °C for the same microwave powers, respectively. It is noteworthy that temperature gradients are also expected in the radial direction, although they have not been measured in this paper. Several papers show this effect in experiments and modelling (Durka et al., 2011; Gangurde et al., 2017; Nigar et al., 2019).

Remarkably, although microwave-assisted desorption was carried out in a multimode microwave cavity, the temperature distribution within the bed was always the same. Namely, the higher the FO sensor was located, the higher the bed temperatures were measured. This effect was observed for all tested samples. Intriguingly, such performance was also observed in our earlier work aimed at microwave heating of water in a monomode applicator (Cherbański and Rudniak, 2013). This previous work showed that a change in the incident microwave power for a fixed frequency only scales absorbed power without affecting the volume loss density distribution or temperature distribution.

Importantly, the regeneration degree was not less than about 80%, even in the case of the lowest applied microwave power (16 W). For the highest tested power of 32 W, 95% regeneration degree was obtained for the ATPC 2 sample. A comparison of the regeneration times in Figs. 7 and 8 also shows that much shorter times were required to regenerate ATPC than GAC. It seems that this difference is mainly related to the maximum amount of adsorption for these adsorbents, which is undoubtedly linked to the development of their internal structure.

As far as we know, this is the first attempt to investigate microwave-assisted regeneration of n-hexane loaded carbonaceous adsorbents. Therefore, a direct discussion of our and literature results is not possible. On the other hand, there are a few articles which report on microwave-assisted regeneration of various VOC loaded carbonaceous adsorbents. For example, Dehdashti et al. (2011) investigated microwave-assisted regeneration of GAC loaded with toluene. The toluene removal was tested in a fixed-bed apparatus containing 10 g of spent GAC. The sample was heated at the microwave powers of 180, 360, 540, 720, and 900 W for 5, 10, 15, 20, and 25 min. The discussion with our results obtained for GAC is possible using microwave energy calculated as the product of microwave power and time. These simple calculations show that the microwave energy of 486 kJ was needed to desorb 90% of toluene within 15 minutes at 540 W in (Dehdashti et al., 2011). A very similar energy of 460 kJ was used to remove n-hexane from the GAC

sample in our experiments. The process yielded about 12% residual n-hexane after irradiation for 250 min at 32 W. Although n-hexane (69 °C) and toluene (110 °C) have different boiling points, our experiments have shown that such temperatures are achieved very fast, even at low microwave powers utilized in the present work (max. 32 W). Therefore, this difference should not have a significant impact on the compared results obtained in this work and in Dehdashti et al. (2011).

Microwave regeneration of beaded activated carbon (BAC) loaded with n-dodecane was investigated by Fayaz et al. (2015). They compared two alternative regeneration methods: microwave heating and conductive heating. The experiments were carried out for different times at a constant applied power of 180 W. Importantly, the results showed that the energy required to attain equal desorption efficiencies was lower for microwave heating in every case. Surprisingly, the regeneration efficiency of 100% was gained using only 56 kJ of microwave energy with power ranging from 100 to 220 W. However, a more careful analysis revealed that specific power of ~34 W/g (5.3 g of BAC) was applied in Fayaz et al. (2015), whereas it was only ~2.4 W/g (13.15 g of GAC) in our work. In addition, microwaves were delivered in an advanced and optimized monomode microwave system with power monitoring in Fayaz et al. (2015), whereas a general purpose microwave reactor with a multimode cavity was used in this work.

The regeneration of spent activated carbons loaded with toluene and acetone was investigated by Mao et al. (2015b). Three regeneration methods were compared: constant power (CPMH), constant temperature (CTMH) microwave heating and conductive heating (CH). For toluene, the researchers found that CPMH and CTMH required 13.5 and 27 kJ/g of microwave energy to achieve almost full regeneration of the adsorbent at 600 W of microwave power, respectively. For acetone, both methods required 4.5 and 9 kJ/g of microwave energy to achieve the same goal at the same microwave power, respectively. They concluded that the two microwave methods were more efficient than CH. Given that ~13 g of GAC was used in our experiments, one can calculate the energies of 175.5 kJ and 58.5 kJ for desorption of toluene and acetone with CPMH, respectively. Importantly, a more careful analysis reveals that a huge power of 75 W per 1 g of adsorbent has been applied in Mao et al. (2015b).

Although the effect of microwave power on microwave energy consumption was not discussed in Mao et al. (2015b), it can be concluded, based on the data from Fig. 3 (Mao et al., 2015b), that it was 5.4, 15.8, 13.5 kJ/g for toluene desorption, and was 3.2, 11.3, 4.5 kJ/g for acetone desorption from pine activated carbon at 60, 300 and 600 W, respectively. In addition, it was 5.4, 9.0, 9.0 kJ/g for toluene desorption, and it was 3.6, 6.8, 4.5 kJ/g for acetone desorption from wheat activated carbon at 60, 300 and 600 W, respectively. Interestingly, this shows that the supplied microwave power should be optimized to minimize microwave energy consumption. In other words, the balance between the supplied microwave power and the power lost to the surroundings is beneficial from the energetic point of view for the mean microwave power. Analysing our results more carefully (see Figs. 8 and 9), one can find that the arbitrary assumed regeneration degree of 80% is reached after 475, 325 and 100 min for the GAC bed at the microwave powers of 16, 24 and 32 W, respectively. For the ATPC bed, the same regeneration degree is achieved after 40, 40, 16 min at the microwave powers of 16, 24 and 32 W, respectively. This shows that the microwave power of 32 W is the most efficient from the energy consumption point of view in our case, giving 192 and 31 kJ (or 14.8 and 2.4 kJ/g) for 80% regeneration of GAC and ATPC, respectively.

As already mentioned, a general purpose microwave reactor with a multimode cavity was used in this work. As a consequence, the microwave heating of our samples was not optimized in any way. To estimate the efficiency of microwave energy conversion into heat in this non-optimized setup, simple calculations were carried out on the basis of the balance equation 14) and the temperature profiles measured for the following samples: GAC 10 (16 W), GAC 11 (24 W), GAC 3 (32 W), ATPC 5 (16 W), ATPC 6 (24 W), ATPC 2 (32 W).

$$\dot{Q}_{\text{gen}} = \dot{Q}_{\text{acc}} + \dot{Q}_{\text{loss}} + \dot{Q}_{\text{gas}} \tag{14}$$

where: $\dot{Q}_{gen}$ is the heat generation rate due to microwaves, $\dot{Q}_{acc}$ is the heat accumulation rate, $\dot{Q}_{loss}$ is the heat loss rate, $\dot{Q}_{gas}$ is the heat withdraw rate due to the purge gas.

The efficiencies of microwave energy conversion into heat was calculated from Equation (15) as the ratio of generated, $\dot{Q}_{gen}$, and irradiated, $\dot{Q}_{MW}$, microwave powers.

$$\eta_{MW\rightarrow heat} = \dot{Q}_{gen}/\dot{Q}_{MW} \cdot 100\% \tag{15}$$

The calculated average efficiencies are in the ranges of 28–39% and 5–6% for the GAC and ATPC samples, respectively.

Figure 9 shows the effect of purge flow rate on desorption. The correlation between the regeneration rate and the purge gas flow rate is obvious for the GAC samples but it has no apparent effect on the ATPC samples. Importantly, the results obtained for GAC reveal that the external mass resistance controls the desorption rate up to the purge flow rate of 300 Nml/min. For the highest purge flow rate of 400 Nml/min, it is very likely that the external mass transfer is removed and the internal diffusion limits the rate of the desorption process, which appears as practically the same regeneration degree profiles for 300 and 400 Nml/min in Fig. 9. In this context, the regeneration times reported in Figs. 7 and 8 would likely be significantly shortened as they are still in the flow range which is limited by the external mass transfer resistance (200 Nml/min). Hopefully, this should decrease microwave energy required to reach the same regeneration levels for our samples.

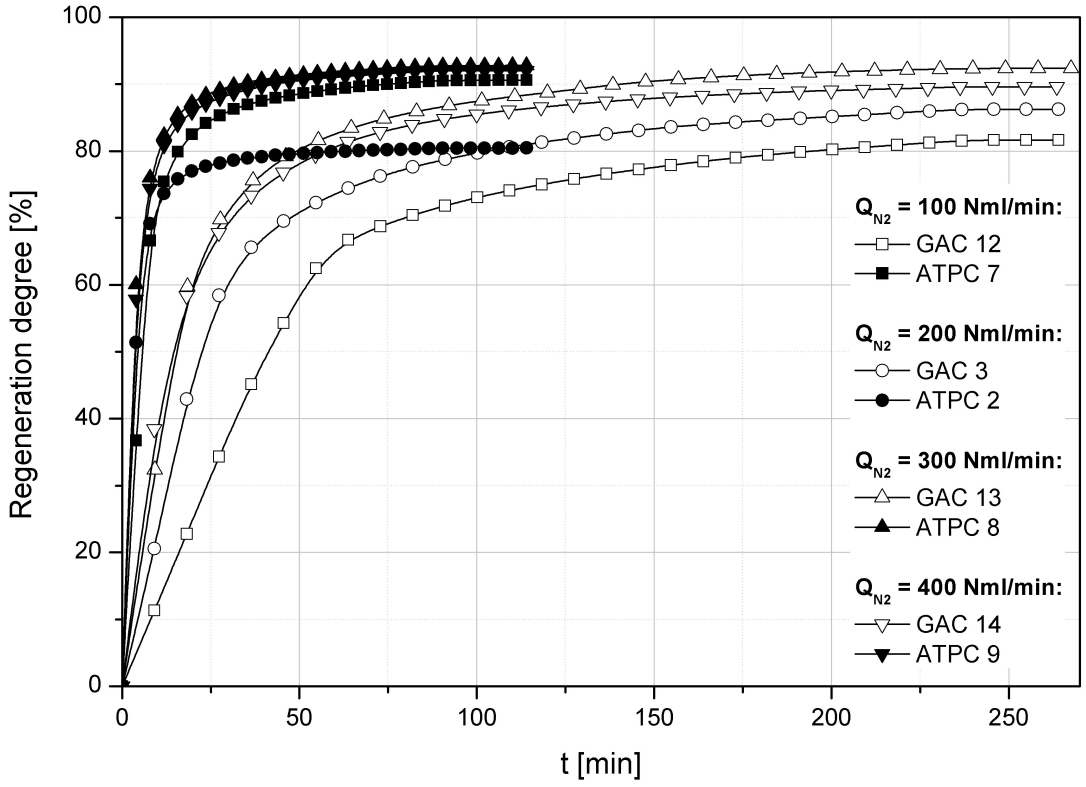

Fig. 9. The effect of purge flow rate on desorption for GAC and ATPC

Figure 10 shows the effect of magnetite (Fe_3O_4) on microwave desorption. Although the results presented are only preliminary, they encourage further research to be undertaken in the future. Note that that small amount of Fe_3O_4 added to the GAC bed slightly improved the regeneration degree. From the practical point of view, magnetite can be separated very easily using a magnet.

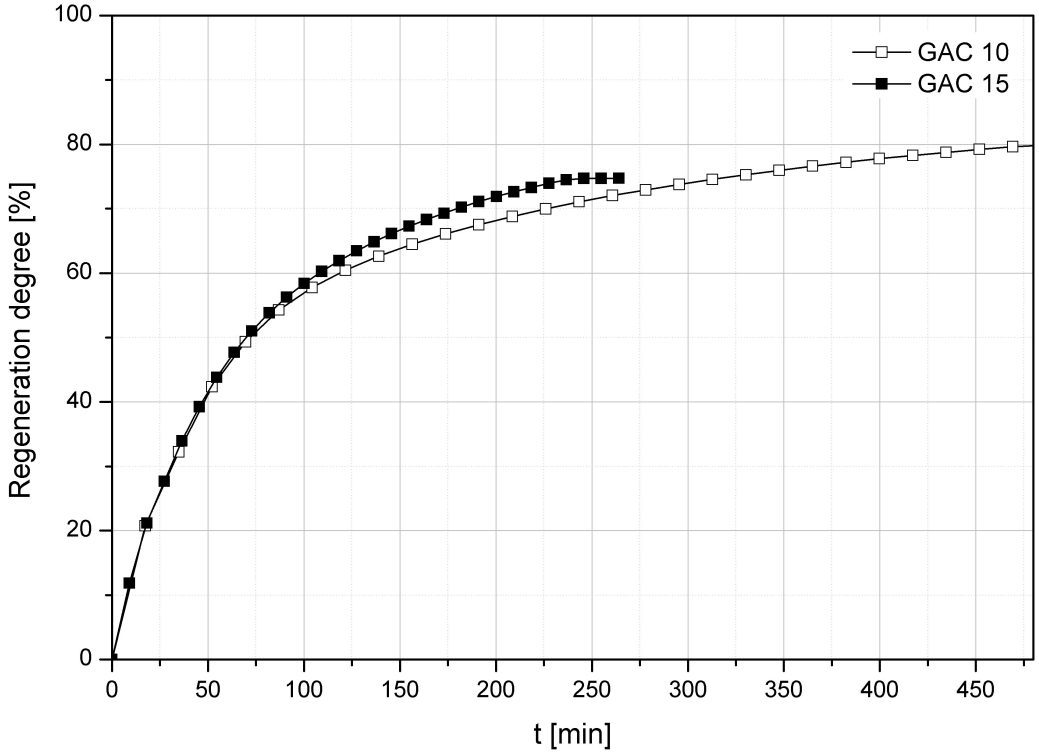

Fig. 10. The effect of magnetite (Fe_3O_4) on desorption

5. CONCLUSIONS

Activated tyre pyrolysis char was tested against a reference GAC as an n-hexane adsorbent. For the both adsorbents, the PFO and PSO models, which are very frequently used to model adsorption kinetics, gave rather disappointing results, showing poor agreement with the experimental data. On the other hand, a good fit with the experimental data was obtained for the family of dynamic adsorption models including the Thomas, Yoon–Nelson and Bohart–Adams models. These three models were successfully introduced using a unified logistic function. In addition, the IP model was employed to check what the rate-limiting step in the adsorption process on GAC and ATPC was. This analysis showed that internal diffusion is probably the rate-limiting step during adsorption on ATPC. On the other hand, the external and internal diffusion plays a role during adsorption on GAC. Based on the obtained breakthrough curves and assuming a 50% breakthrough time corresponding to the ratio $C/C_0 = 0.5$, the gas volumes that can be purified with ATPC and GAC are in the range from 20–90 cm^3/g to 935–1240 cm^3/g, respectively. Although the maximum adsorbed amount of n-hexane on ATPC was 20% of that for GAC, it should be noted that the adsorption properties of ATPC can be significantly improved by its chemical activation (Kuśmierek et al., 2020a). Both adsorbent proved to be suitable for microwave-assisted regeneration, showing very fast heating rates even at low microwave powers. The presented preliminary results with the use of microwave susceptor (Fe_3O_4) showed that microwave-assisted regeneration has the potential to further reduce microwave energy consumption.

SYMBOLS

A	constant in the corelation for Sherwood number, –
a	the coefficient in Equation (6) (logistic function), –

$Area$	the chromatographic response of the FID detector, mV·min
$Area_{MAX}$	the maximum signal of FID detector for the loaded adsorbent, mV·min
b	the coefficient in Equation (6) (logistic function), min^{-1}
C	the constant connected with the boundary layer thickness (i.e. the film thickness for the external film diffusion model), $mg \cdot g^{-1}$
C_0	the concentration of n-hexane in inlet stream to column, $mg \cdot ml^{-1}$
C_t	the concentration of n-hexane in outlet stream from column at time t, $mg \cdot ml^{-1}$
D_{AB}	the diffusion coefficient, $m^2 \cdot s^{-1}$
df	the degree of freedom, –
d_h	the hydraulic diameter of particles, m
e	constant in the corelation for Sherwood number, –
f	constant in the corelation for Sherwood number, –
K	the proportional constant between the mass transfer coefficient k_c and velocity of gas u_0, $(m \cdot s^{-1})^{1-e}$
k_{BA}	the Bohart–Adams rate constant, $ml \cdot mg^{-1} \cdot min^{-1}$
k_c	the mass transfer coefficient, $m \cdot s^{-1}$
K_p	the IP model rate constant, $mg \cdot g^{-1} \cdot s^{0.5}$
k_{Th}	the Thomas rate constant, $ml \cdot mg^{-1} \cdot min^{-1}$
k_{YN}	the Yoon–Nelson rate constant, min^{-1}
k_1	the pseudo-first order rate constant, min^{-1}
k_2	the pseudo-second order rate constant, $g \cdot mg^{-1} \cdot min^{-1}$
k_2^*	the product of k_2 and q_e, min^{-1}
m	the amount of absorbent in the column, g
$m_{ads}(t)$	the adsorbed mass of n-hexane at the time t, g
$m_{hex,ads}^{GC}$	the adsorbed mass of n-hexane (calculated according to chromatography data), g
$m_{hex,ads}^{weight}$	the adsorbed mass of n-hexane (calculated according to weigh), g
$m_{des}(t)$	the desorbed mass of n-hexane at the time t, g
N_0	the adsorptive capacity of the adsorbent, $mg \cdot ml^{-1}$
$Slope$	the slope of the calibration curve, $g/(cm^3 \cdot mV \cdot min)$
V	the superficial velocity of eluent, $cm \cdot min^{-1}$
ν	the kinematic viscosity of gas phase, $m^2 \cdot s^{-1}$
$\dot{V}_{N_2}^{273.15}$	the volumetric flow rate of the carrier/purge gas (N_2) at the normal temperature (displayed on the mass flow controller), Nml/min
Q	the vapour flow rate, $ml \cdot min^{-1}$
$\dot{Q}_{acc}$	the heat accumulation rate, W
$\dot{Q}_{gen}$	the heat generation rate due to microwaves, W
$\dot{Q}_{gas}$	the heat withdraw rate due to the purge gas, W
$\dot{Q}_{loss}$	the heat loss rate, W
q	the amount of adsorbed n-hexane per unit mass of adsorbent, $mg \cdot g^{-1}$
$q(t)$	the amount of adsorbed n-hexane per unit mass of adsorbent at time t, $mg \cdot g^{-1}$
q_e	the amount of adsorbed n-hexane per unit mass of adsorbent at equilibrium, $mg \cdot g^{-1}$
$\overline{R}^2$	the adjusted coefficient of determination, –
Re	Reynolds number, –
RSS	the residual sum of squares, –
RelError	the relative error, %
Sc	Schmidt number, –

Sh	Sherwood number, –
t	the time, min
TSS	the total sum of squares, –
u_0	the superficial velocity, $m \cdot s^{-1}$
X	the bed height, cm

Greek symbols

$\eta_{MW \rightarrow heat}$	the efficiency of microwave energy conversion into heat, %
τ	the time required to reach $C_t/C_0 = 0.5$, parameter of the Yoon–Nelson model, min

REFERENCES

Acosta R., Fierro V., Martinez de Yuso A., Nabarlatz D., Celzard A., 2016. Tetracycline adsorption onto activated carbons produced by KOH activation of tyre pyrolysis char. *Chemosphere*, 149, 168–176. DOI: 10.1016/j.chemosphere.2016.01.093.

Ania C.O., Menéndez J.A., Parra J.B., Pis J.J., 2004. Microwave-induced regeneration of activated carbons polluted with phenol. A comparison with conventional thermal regeneration. *Carbon*, 42, 1383–1387. DOI: 10.1016/j.carbon.2004.01.010.

Ania C.O., Parra J.B., Menéndez J.A., Pis J.J., 2005. Effect of microwave and conventional regeneration on the microporous and mesoporous network and on the adsorptive capacity of activated carbons. *Microporous Mesoporous Mater.*, 85, 7–15. DOI: 10.1016/j.micromeso.2005.06.013.

Ania C.O., Parra J.B., Menéndez J.A., Pis J.J., 2007. Microwave-assisted regeneration of activated carbons loaded with pharmaceuticals. *Water Res.*, 41, 3299–3306. DOI: 10.1016/j.watres.2007.05.006

Antoniou N., Stavropoulos G., Zabaniotou A., 2014. Activation of end of life tyres pyrolytic char for enhancing viability of pyrolysis – Critical review, analysis and recommendations for a hybrid dual system. *Renewable Sustainable Energy Rev.*, 39, 1053–1073. DOI: 10.1016/j.rser.2014.07.143.

Bathen D., 2003. Physical waves in adsorption technology – an overview. *Sep. Purif. Technol.*, 33, 163–177. DOI: 10.1016/S1383-5866(03)00004-2.

Bohart G.S., Adams E.Q., 1920. Some aspects of the behavior of charcaol with respect to chlorine. *J. Am. Chem. Soc.*, 42, 523–544. DOI: 10.1021/ja01448a018.

Burkholder H. R., Fanslow G. E. , Bluhm D., 1986. Recovery of ethanol from a molecular sieve by using dielectric heating. *Ind. Eng. Chem. Fundam.*, 25, 414–416. DOI: 10.1021/i100023a019.

Çalişkan E., Bermúdez J.M., Parra J.B., Menéndez J.A., Mahramanlıoğlu M., Ania C.O., 2012. Low temperature regeneration of activated carbons using microwaves: Revising conventional wisdom. *J. Environ. Manage.*, 102, 134–140. DOI: 10.1016/j.jenvman.2012.02.016.

Cha C.Y., Carlisle C.T., 2001. Microwave process for volatile organic compound abatement. *J. Air Waste Manage. Assoc.*, 51, 1628–1641. DOI: 10.1080/10473289.2001.10464389.

Cha C.Y., Wallace S., George A.H., Rogers S., 2004. Microwave Technology for Treatment of Fume Hood Exhaust. *J. Envirnomental Eng.*, 130, 338–348. DOI: 10.1061/(ASCE)0733-9372(2004)130:3(338).

Chatterjee A., Schiewer S., 2011. Biosorption of cadmium(II) ions by citrus peels in a packed bed column: Effect of process parameters and comparison of different breakthrough curve models. *CLEAN – Soil Air Water*, 39, 874–881. DOI: 10.1002/clen.201000482.

Cherbański R., 2018. Regeneration of granular activated carbon loaded with toluene – Comparison of microwave and conductive heating at the same active powers. *Chem. Eng. Process. Process Intensif.*, 123, 148–157. DOI: 10.1016/j.cep.2017.11.008.

Cherbański R., Komorowska-Durka M., Stefanidis G.D., Stankiewicz A.I., 2011. Microwave swing regeneration vs temperature swing regeneration – Comparison of desorption kinetics. *Ind. Eng. Chem. Res.*, 50, 8632–8644. DOI: 10.1021/ie102490v.

Cherbański R., Molga E., 2009. Intensification of desorption processes by use of microwaves – An overview of possible applications and industrial perspectives. *Chem. Eng. Process. Process Intensif.*, 48, 48–58. DOI: 10.1016/j.cep.2008.01.004.

Cherbański R., Rudniak L., 2013. Modelling of microwave heating of water in a monomode applicator – Influence of operating conditions. *Int. J. Therm. Sci.*, 74, 214–229. DOI: 10.1016/j.ijthermalsci.2013.07.001.

Chu K.H., 2020. Breakthrough curve analysis by simplistic models of fixed bed adsorption: In defense of the century-old Bohart–Adams model. *Chem. Eng. J.*, 380, 122513. DOI: 10.1016/j.cej.2019.122513.

Clean Air Technology E.P.A., 1999. Choosing an adsorption system for VOC: carbon, zeolite or polymers? *CATC Tech. Bull.*, EPA-456/F-99-004. Available at: https://www3.epa.gov/ttncatc1/dir1/fadsorb.pdf.

Coss P.M., Cha C.Y., 2000. Microwave regeneration of activated carbon used for removal of solvents from vented air. *J. Air Waste Manage. Assoc.*, 50, 529–535. DOI: 10.1080/10473289.2000.10464038.

Dehdashti A., Khavanin A., Rezaee A., Asilian H., 2011. Regeneration of granular activated carbon saturated with gaseous toluene by microwave irradiation. *Turkish J. Eng. Env. Sci.*, 35, 49–58. DOI: 10.3906/muh-1004-13.

Directive 2004/42/CE of the European Parliament and of the Council of 21 April 2004 on the limitation of emissions of volatile organic compounds due to the use of organic solvents in certain paints and varnishes and vehicle refinishing products and amendi Directive 1999/13/EC. *Off. J. L.*, 143, 87–96.

Directive 2010/75/EU of the European Parliament and of the Council of 24 November 2010 on industrial emissions (integrated pollution prevention and control). *Off. J. L.*, 334, 17–119.

Durka T., Stefanidis G.D., Van Gerven T., Stankiewicz A.I., 2011. Microwave-activated methanol steam reforming for hydrogen production. *Int. J. Hydrog. Energy*, 36, 12843–12852. DOI: 10.1016/j.ijhydene.2011.07.009.

ETRMA, 2019. *End of Life Tyres Management – Europe – 2017*. Brussels, 19.11.2019.

Fayaz M., Shariaty P., Atkinson J.D., Hashisho Z., Phillips J. H., Anderson J.E., Nichols M., 2015. Using microwave heating to improve the desorption efficiency of high molecular weight VOC from beaded activated carbon. *Environ. Sci. Technol.*, 49, 4536–4542. DOI: 10.1021/es505953c.

Foo K.Y., Hameed B.H., 2012a. A cost effective method for regeneration of durian shell and jackfruit peel activated carbons by microwave irradiation. *Chem. Eng. J.*, 193–194, 404–409. DOI: 10.1016/j.cej.2012.04.055.

Foo K.Y., Hameed B.H., 2012b. A rapid regeneration of methylene blue dye-loaded activated carbons with microwave heating. *J. Anal. Appl. Pyrolysis*, 98, 123–128. DOI: 10.1016/j.jaap.2012.07.006.

Foo K.Y., Hameed B.H., 2012c. Microwave-assisted regeneration of activated carbon. *Bioresour. Technol.*, 119, 234–240. DOI: 10.1016/j.biortech.2012.05.061.

Gangurde L.S., Sturm G.S.J., Devadiga T.J., Stankiewicz A.I., Stefanidis G.D., 2017. Complexity and challenges in noncontact high temperature measurements in microwave-assisted catalytic reactors. *Ind. Eng. Chem. Res.*, 56, 13379–13391. DOI: 10.1021/acs.iecr.7b02091.

Han R., Wang Y., Sun Q., Wang L., Song J., He X., Dou C., 2010. Malachite green adsorption onto natural zeolite and reuse by microwave irradiation. *J. Hazard. Mater.*, 175, 1056–1061. DOI: 10.1016/j.jhazmat.2009.10.118.

Han Z., Kong S., Sui H., Li X., Zhang Z., 2019. Preparation of carbon-silicon doping composite adsorbent material for removal of VOCs. *Materials*, 12, 2438. DOI: 10.3390/ma12152438.

Hashisho Z., Rood M., Botich L., 2005. Microwave-swing adsorption to capture and recover vapors from air streams with activated carbon fiber cloth. *Environ. Sci. Technol.*, 39, 6851–6859. DOI: 10.1021/es050338z.

Hubbe M.A., Azizian S., Douven S., 2019. Implications of apparent pseudo-second-order adsorption kinetics onto cellulosic materials: A review. *BioRes.*, 14, 7582–7626.

Kandasamy J., Gokalp I., 2015. Pyrolysis, combustion, and steam gasification of various types of scrap tires for energy recovery. *Energy Fuels*, 29, 346–354. DOI: 10.1021/ef502283s.

Kim K.J., Ahn H.G., 2012. The effect of pore structure of zeolite on the adsorption of VOCs and their desorption properties by microwave heating. *Microporous Mesoporous Mater.*, 152, 78–83. DOI: 10.1016/j.micromeso.2011.11.051.

Kim K.J., Kim Y.H., Jeong W.J., Park N.-C., Jeong S.-W., Ahna H.-G., 2007. Adsorption-desorption characteristics of volatile organic compounds over various zeolites and their regeneration by microwave irradiation. *Stud. Surf. Sci. Catal.*, 165, 223–226. DOI: 10.1016/S0167-2991(07)80304-1.

Kotkowski T., Cherbański R., Molga E., 2018. Acetone adsorption on CO_2-activated tyre pyrolysis char – Thermogravimetric analysis. *Chem. Process Eng.*, 39, 233–246. DOI: 10.24425/122946.

Kotkowski T., Cherbański R., Molga E., 2020. Tyre-derived activated carbon – textural properties and modelling of adsorption equilibrium of n-hexane. *Chem. Process Eng.*, 41, 25–44. DOI: 10.24425/cpe.2019.130221.

Kuśmierek K., Świątkowski A., Kotkowski T., Cherbański R., Molga E., 2020a. Adsorption of bisphenol a from aqueous solutions by activated tyre pyrolysis char – Effect of physical and chemical activation. *Chem. Process Eng.*, 41, 129–141. DOI: 10.24425/cpe.2020.132536.

Kuśmierek K., Świątkowski A., Kotkowski T., Cherbański R., Molga E., 2020b. Adsorption properties of activated tire pyrolysis chars for phenol and chlorophenols. *Chem. Eng. Technol.*, 43, 770–780. DOI: 10.1002/ceat.201900574.

Kuśmierek K., Świątkowski A., Kotkowski T., Cherbański R., Molga E., 2021a. Adsorption on activated carbons from end-of-life tyre pyrolysis for environmental applications. Part I. Preparation of adsorbent and adsorption from gas phase. *J. Anal. Appl. Pyrolysis*, 157, 105205. DOI: 10.1016/j.jaap.2021.105205.

Kuśmierek K., Świątkowski A., Kotkowski T., Cherbański R., Molga E., 2021b. Adsorption on activated carbons from end-of-life tyre pyrolysis for environmental applications. Part II. Adsorption from aqueous phase. *J. Anal. Appl. Pyrolysis*, 158, 105206. DOI: 10.1016/j.jaap.2021.105206.

Lagergren S., 1898. About the theory of so-called adsorption of soluble substances. *Handlingar*, 24, 1–39.

Liu X., Quan X., Bo L., Chen S., Zhao Y., 2004. Simultaneous pentachlorophenol decomposition and granular activated carbon regeneration assisted by microwave irradiation. *Carbon*, 42, 415–422. DOI: 10.1016/j.carbon.2003.12.032.

López G., Olazar M., Artetxe M., Amutio M., Elordi G., Bilbao J., 2009. Steam activation of pyrolytic tyre char at different temperatures. *J. Anal. Appl. Pyrolysis*, 85, 539–543. DOI: 10.1016/j.jaap.2008.11.002.

Mao H., Zhou D., Hashisho Z., Wang S., Chen H., Wang H. H., Lashaki M. J., 2015a. Microporous activated carbon from pinewood and wheat straw by microwave-assisted KOH treatment for the adsorption of toluene and acetone vapors. *RSC Adv.*, 5, 36051–36058. DOI: 10.1039/C5RA01320H.

Mao H., Zhou D., Hashisho Z., Wang S., Chen H., Wang H.H., 2015b. Constant power and constant temperature microwave regeneration of toluene and acetone loaded on microporous activated carbon from agricultural residue. *J. Ind. Eng. Chem.*, 21, 516–525. DOI: 10.1016/j.jiec.2014.03.014.

Meier M., Turner M., Vallee S., Conner W.C., Lee K.H., Yngvesson K.S., 2009. Microwave regeneration of zeolites in a 1 meter column. *AIChE J.*, 55, 1906–1913. DOI: 10.1002/aic.11793.

Mui E.L.K., Ko D.C.K., McKay G., 2004. Production of active carbons from waste tyres – a review. *Carbon*, 42, 2789–2805. DOI: 10.1016/j.carbon.2004.06.023.

Nigar H., Sturm G.S.J., Garcia-Baños B., Peñaranda-Foix F.L., Catalá-Civera J.M., Mallada R., Stankiewicz A., Santamaría J., 2019. Numerical analysis of microwave heating cavity: Combining electromagnetic energy, heat transfer and fluid dynamics for a NaY zeolite fixed-bed. *Appl. Therm. Eng.*, 155, 226–238. DOI: 10.1016/j.applthermaleng.2019.03.117.

OriginLab Corporation, 2021. *OriginPro 8 SR0*.

Plazinski W., Rudzinski W., Plazinska A., 2009. Theoretical models of sorption kinetics including a surface reaction mechanism: A review. *Adv. Colloid Interface Sci.*, 152, 2–13. DOI: 10.1016/j.cis.2009.07.009.

Polaert I., Estel L., Huyghe R., Thomas M., 2010. Adsorbents regeneration under microwave irradiation for dehydration and volatile organic compounds gas treatment. *Chem. Eng. J.*, 162, 941–948. DOI: 10.1016/j.cej.2010.06.047.

Price D.W., Schmidt P.S., 1998. VOC recovery through microwave regeneration of adsorbents: Process design studies. *J. Air Waste Manage. Assoc.*, 48, 1135–1145. DOI: 10.1080/10473289.1998.10463758.

Quan X., Liu X., Bo L., Chen S., Zhao Y., Cui X., 2004. Regeneration of acid orange 7-exhausted granular activated carbons with microwave irradiation. *Water Res.*, 38, 4484–4490. DOI: 10.1016/j.watres.2004.08.031.

Reuß J., Bathen D., Schmidt-Traub H., 2002. Desorption by microwaves: Mechanisms of multicomponent mixtures. *Chem. Eng. Technol.*, 25, 381–384. DOI: 10.1002/1521-4125(200204)25:4<381::AID-CEAT381>3.0.CO;2-0.

Robers A., Figura M., Thiesen P.H., Niemeyer B., 2005. Desorption of odor-active compounds by microwaves, ultrasound, and water. *AIChE J.*, 51, 502–510. DOI: 10.1002/aic.10334.

Roussy G., Chenot P., 1981. Selective energy supply to adsorbed water and nonclassical thermal process during microwave dehydration of zeolite. *J. Phys. Chem.*, 85, 2199–2203. DOI: 10.1021/j150615a013.

Roussy G., Zoulalian A., Charreyre M., Thiebaut J.-M., 1984. How microwaves dehydrate zeolites. *J. Phys. Chem.*, 88, 5702–5708. DOI: 10.1021/j150667a049.

Rudzinski W., Plazinski W., 2007. Studies of the kinetics of solute adsorption at solid/solution interfaces: On the possibility of distinguishing between the diffusional and the surface reaction kinetic models by studying the pseudo-first-order kinetics. *J. Phys. Chem. C*, 111, 15100–15110. DOI: 10.1021/jp073249c.

Sharma V.K., Mincarini M., Fortuna F., Cognini F., Cornacchia G., 1998. Disposal of waste tyres for energy recovery and safe environment–Review. *Energy Convers. Manage.*, 39, 511–528. DOI: 10.1016/S0196-8904(97)00044-7.

Sienkiewicz M., Kucinska-Lipka J., Janik H., Balas A., 2012. Progress in used tyres management in the European Union: A review. *Waste Manage.*, 32, 1742–1751. DOI: 10.1016/j.wasman.2012.05.010.

Simonin J.P., 2016. On the comparison of pseudo-first order and pseudo-second order rate laws in the modeling of adsorption kinetics. *Chem. Eng. J.*, 300, 254–263. DOI: 10.1016/j.cej.2016.04.079.

Stankiewicz A.I., Nigar H., 2020. Beyond electrolysis: old challenges and new concepts of electricity-driven chemical reactors. *React. Chem. Eng.*, 5, 1005–1016. DOI: 10.1039/d0re00116c.

Tan K.L., Hameed B.H., 2017. Insight into the adsorption kinetics models for the removal of contaminants from aqueous solutions. *J. Taiwan Inst. Chem. Eng.*, 74, 25–48. DOI: 10.1016/J.JTICE.2017.01.024.

Wang S., Huang L., Zhang Y., Li L., Lu X., 2021. A mini-review on the modeling of volatile organic compound adsorption in activated carbons: Equilibrium, dynamics, and heat effects. *Chin. J. Chem. Eng.*, 31, 153–163. DOI: 10.1016/j.cjche.2020.11.018.

Wang W., Li M., Zeng Q., 2015. Adsorption of chromium (VI) by strong alkaline anion exchange fiber in a fixed-bed column: Experiments and models fitting and evaluating. *Sep. Purif. Technol.*, 149, 16–23. DOI: 10.1016/j.seppur.2015.05.022.

Weber W.J., Morris J.C., 1963. Kinetics of Adsorption on Carbon from Solution. *J. Sanit. Eng. Div.*, 89, 31–59. DOI: 10.1061/JSEDAI.0000430.

Witkiewicz K., Nastaj J., 2014. Modeling of microwave-assisted regeneration of selected adsorbents loaded with water or toluene. *Drying Technol.*, 32, 1369–1385. DOI: 10.1080/07373937.2014.900506.

World Business Council for Sustainable Development, 2008. *Managing End-of-Life Tires*. Available at: https://www.wbcsd.org/Sector-Projects/Tire-Industry-Project/Resources/Managing-End-of-Life-Tires.

Wu F.C., Tseng R.L., Juang R.S., 2009. Initial behavior of intraparticle diffusion model used in the description of adsorption kinetics. *Chem. Eng. J.*, 153, 1–8. DOI: 10.1016/j.cej.2009.04.042.

Yan J., Xue Y., Long L., Zeng Y., Hu X., 2018. Adsorptive removal of As(V) by crawfish shell biochar: batch and column tests. *Environ. Sci. Pollut. Res.*, 25, 34674–34683. DOI: 10.1007/s11356-018-3384-1.

Yang Z., Yi H., Tang X., ZhaoS., Yu Q., Gao F., Zhou Y., Wang J., Huang Y., Yang K., Shi Y., 2017. Potential demonstrations of "hot spots" presence by adsorption-desorption of toluene vapor onto granular activated carbon under microwave radiation. *Chem. Eng. J.*, 319, 191–199. DOI: 10.1016/j.cej.2017.02.157.

Yoon Y.H. , Nelson J.H., 1984. Application of Gas Adsorption Kinetics I. A Theoretical Model for Respirator Cartridge Service Life. *Am. Ind. Hyg. Assoc. J.*, 45, 509–516. DOI: 10.1080/15298668491400197.

Yuen F.K., Hameed B.H., 2009. Recent developments in the preparation and regeneration of activated carbons by microwaves. *Adv. Colloid Interface Sci.*, 149, 19–27. DOI: 10.1016/j.cis.2008.12.005.

Zhang D., Cao J., Wu G., Cui L., 2018. Dynamic adsorption model fitting studies of typical VOCs using commercial activated carbon in a fixed bed. *Water Air Soil Pollut.*, 229, 178. DOI: 10.1007/s11270-018-3763-8.

Received 10 December 2021
Received in revised form 21 February 2022
Accepted 01 March 2022